JOURNAL OF MATERIALS SCIENCE **40** (2005) 1709– 1715

Examination of morphological changes of pore channel network during the intermediate stage of sintering of undoped, MgO-doped and ZrO_2-doped alumina compacts by modified statistical theory of sintering

TSANG-TSE FANG, FUH-SHAN SHIAU
Department of Materials Science and Engineering, National Cheng Kung University, Tainan 701, Taiwan

The modified statistical theory of sintering was used to evaluate the microstructural parameters, such as the average pore radius, grain size, and total length per unit volume of pore, of undoped and doped alumina compacts during the intermediate stage of sintering. The present results further justify the validity of the modified statistical theory of sintering in characterizing the morphological changes of pore channel network. The evaluated data of the evolution of these morphological parameters provide deep insight of the understanding of the mechanism of the effects of particle size distributions, MgO and ZrO_2 on breakup of pore channel network. The possible roles of MgO and ZrO_2 in the intermediate stage of sintering have been discussed.

1. Introduction

Sintering is a very complicated process, which involves the simultaneously morphological changes of pores and grains through the action of several different transport mechanisms. It has been practically modeled as three stages, i.e., initial, intermediate, and final stages [1]. Models of the initial stage of sintering were pursued more intensely early in the sintering field, which provided not only an understanding of the fundamental theory of sintering but also the evaluation of reasonably accurate values of diffusivities. However, it faded in interest because essentially, the control of the microstructure is determined by the later stages of sintering. The final stage of sintering has drawn the most attention because it is at this stage where most properties of practical interest are realized. Basically, there are two approaches for the final-stage sintering models. One approach was quantitatively to determine the sintering kinetics. Another approach is to develop the density-grain size trajectory for the understanding of the microstructural evolution [2–11]. Based on these studies, the pore morphology and location were recognized to play a significant role in the microstructural evolution, which however, is determined by the morphological changes of the pore channel network in the intermediate stage of sintering [12].

The intermediate stage of sintering was relatively less studied than the other two stages, which might be due to its more complicated pore morphology. Most intermediate stage sintering models [1, 13–16]. focused on the studies related to the sintering kinetics or transport mechanisms. By contrast, there were a few reports on the morphological evolution of the pore channel network [17, 18]. Several simplified models using artificial pore channels or cracking-like flaws have suggested that perturbation phenomena of the type described by Rayleigh [19] and others [20–27] not only was applicable to but also provided useful information for the breakup mechanism of the pore channel in powder compacts undergoing densification. However, in a real powder compact, the connective network and pore size distribution would complicate this phenomenon, therefore, the use of a model approaching the reality is favorable. Among the intermediate stage sintering models, the modified statistical theory of sintering [18] is capable to meet this requirement. This theory can practically evaluate the microstructural evolution parameters of the powder compacts during sintering based on only the densification rate extracted from the data measured from the dilatometer without destroying the sample. Moreover, it has been successfully applied to the materials of alumina [28] and barium titanate [29].

Regarding the effects of impurity on the sintering behavior of a powder compact, MgO has been intensively investigated [4, 30–52]. MgO in the alumina was usually considered in a form of a solid solution rather than an inclusion. Most reports [4, 30–52] in the literature related to the MgO dopant in alumina were focused on the final stage of sintering though a few [26, 27] on the breakup of pore channels were presented. As for the effect of ZrO_2 dopant in sintering alumina, a few reports [53–57] were presented in the literature and ZrO_2

was usually in a form of an inclusion rather than a solid solution.

In this paper, the modified statistical theory of sintering [18] will be used to evaluate the microstructural evolution parameters in the intermediate stage of sintering of undoped alumina with different particle size distributions and doped alumina with MgO and ZrO_2. Based on these data, it would provide a deep insight about the effect of particle size distribution and dopants of MgO and ZrO_2 on the evolution of the pore channel network during the intermediate stage of sintering.

2. Experimental procedure

A high-purity α-Al_2O_3 powder (AKP-50, Sumitomo Chemical Co., Ltd., Tokyo, Japan) was used throughout this investigation. The classified powders were produced from as-received powders, using the centrifugal process, which began with a slurry of 20 vol% solids dispersed in deionized water that was stabilized at pH 4 with nitric acid. The dispersed slurry was centrifuged at 800 rotations per minute (rpm) for 30 min. Thereafter, the upper-suspension solution of the slurry was further centrifuged at a higher speed up to 2400 rpm. The classified powders were the final sediment in the slurry. The characterization of the particle morphologies of as-received and classified powders has been detailed in the previous work [12]. Magnesia doping (200 ppm) and zirconium doping (400 ppm) were achieved by adding aqueous solutions of $Mg(NO_3)_2$ and $Zr(NO_3)_4$ to the classified powder slurry. The compacts used for studying the sintering kinetics were prepared by slip casting using a high-purity alumina mold to avoid contamination. The compacts were 1.2 cm in diameter and 0.3 cm in thickness.

All compacts were sintered in air at a rate of 10°C/min using fully computerized dilatometer (Model DHT 2050KN, Setaram, Caluire, France). The green and sintered densities were measured by the geometric method and the Archimedes method with distilled, deionized water as the fluid medium, respectively. The value of 3.986 g/cm^3 was used as the theoretical density. All sintered samples were sectioned, ground, polished, and thermally etched to prepare samples for scanning electron microscopy (SEM). The micrographs of SEM were used to evaluate the grain sizes of the sintered bodies. The ASTM intercept method [58] was used to measure the grain size, and circular test lines were used to evaluate more than 300 grains to obtain the average grain size.

The pore morphology was characterized by mercury porosimetry (Model Auto Pore II 9215, Micromeritics Instrument Corp., Norcross, GA). For measurements, the pressure was increased to 414 MPa in 126 steps, with the final pressure corresponding to a pore diameter of 3.2 nm. At each step, the pressure was held for 5 s beyond the time at which no further change in pressure was observed. The maximum intrusion volume used in these measurements was between 30 and 70%. A mercury surface tension of 475 erg/cm^2 and a contact angle of 130° were used in the measurements.

The total length per unit volume of pores, at a given density, was evaluated by mercury porosimetry. The pore shape was assumed to be cylindrical. We also assumed that each cylinder had a mean pore radius of r_i and a length of L_i, therefore, the incremental mercury volume (δV_i) would equal $\pi r_i^2 L_i$. The total length (L) of all pore channels was the sum of L_i for different r_i values; i.e., $L = \Sigma L_i$. The value of L_v, the total length of pore channels per unit volume, was obtained by dividing L by the total volume of the sample.

The theoretical values of the microstructural parameters such as average pore size (r), total length of pores per unit volume (L_v), and average grain size (a) can be evaluated by the morphological kinetic equation developed in the modified statistical theory of sintering [18]. The morphological kinetic equation may be rewritten in the form

$$\ln(\dot{\varepsilon}T) + (Q/R)(1/T) = \ln[(\gamma/k)D^* A_i F_i(y, Z)] + m_i \ln(p/p_o) i/1, 2 \quad (1)$$

where $\dot{\varepsilon}$ is the densification rate, D^* the diffusion constant, γ the surface energy, Q the activation energy, and k the Boltzmann's constant. The intercept parameter, A, is a function of the initial condition of each stage, while the morphological terms, m and y, are related to morphological parameter, x, and pore-size distribution, respectively. Z represents the fraction of active (i.e., shrinking) pores. The subscripts, 1 and 2, represent the intermediate and final stages of sintering, respectively. The m values can be obtained from the slope of Equation 1 by assuming the linearity over a very short time interval in this equation discussed in the previous work [28, 29]. Because the exponent s in Zener's equation [59] ($a = kr/p^s$, where a is the grain size, k the constant, r the pore size, and p the porosity) has been experimentally determined as 0.74 and 0.46 for classified and as-received powder compacts, respectively [60], the values of x can be calculated from the relationships: $x = (m - 0.48)/3$ for the classified powder compacts and $x = (m + 0.08)/3$ for the as-received powder compacts. After determining the values of x, the values of the microstructural parameters such as the average pore size (r), total length of pores per unit volume (L_v), and the average grain size (a) can be evaluated by the following equations

$$r = r_o(p/p_o)^{(1-x)/2}, \quad (2)$$

$$L_v = L_v^o(p/p_o)^x \quad (3)$$

and

$$(a/a_o)(p/p_o)^{s'} = 1, \quad (4)$$

where $s' = s - (1 - x)/2$.

The procedure for determining the onset points of the porosity (p_o) had been detailed in refs. 28 and 29. The initial values of the microstructural parameters r_o, L_v^o, and a_o were experimentally measured at p_o.

3. Results

It is known that diffusion mechanisms of grain boundary and lattice contribute either simultaneously or dominantly to the densification during sintering. However, it is very difficult to take both diffusion mechanisms simultaneously into account in the sintering model, so the individual grain-boundary or lattice diffusion coefficient would be used for the assessment. Moreover, because recent work [61] had shown that the evaluated activation energy for the nonisothermal sintering depended on the heating rates, the values of the activation energies of the grain-boundary and lattice diffusion of the aluminum ion in alumina were taken from the creep data ($8.60 \times 10^{-4}\exp(-418/RT)$ cm^2/s for grain-boundary diffusion and $1.36 \times 10^{5}\exp(-577/RT)$ cm^2/s for lattice diffusion) [62] to exclude factors of heating rate and densification.

Figs 1–3 show comparisons of the experimental and evaluated data of morphological parameters, i.e., r, L_v, and a, of as-received and classified powder compacts, in which the individual lattice or grain-boundary diffusion coefficient was used for the assessment. Based on the observation of Figs 1–3, the consistency between the experimental and evaluated data further demonstrates that the modified statistical theory of sintering [18] is valid to evaluate these parameters of the microstructural evolution and can discern the sintering behaviors of powder compacts with different particle size distributions. Moreover, it should be noted that the evaluated data with lattice diffusion have a better fit to the experimental data. The experimental data in Figs 1–3 had been interpreted and discussed explicitly in ref. 12. However, an insight about L_v and a can be gained from the theoretical data. Because the experimental data using mercury porosimetry would become inaccurate or cannot be measured further when the breakup of channel pores occurs, the theoretical data become favorable and could show a clearer tendency. In Fig. 2, for the as-received powder compact, the evaluated values of L_v showed a clearer quick reduction at relative densities >86%, which is consistent with the observation of the region of the gradual reduction of some open pores in Fig. 4. Moreover, it is more obvious to reveal that the quick reduction of L_v values at relative density 86% is related to the onset of the rapid growth of grains of the as-received compact shown in Fig. 3a.

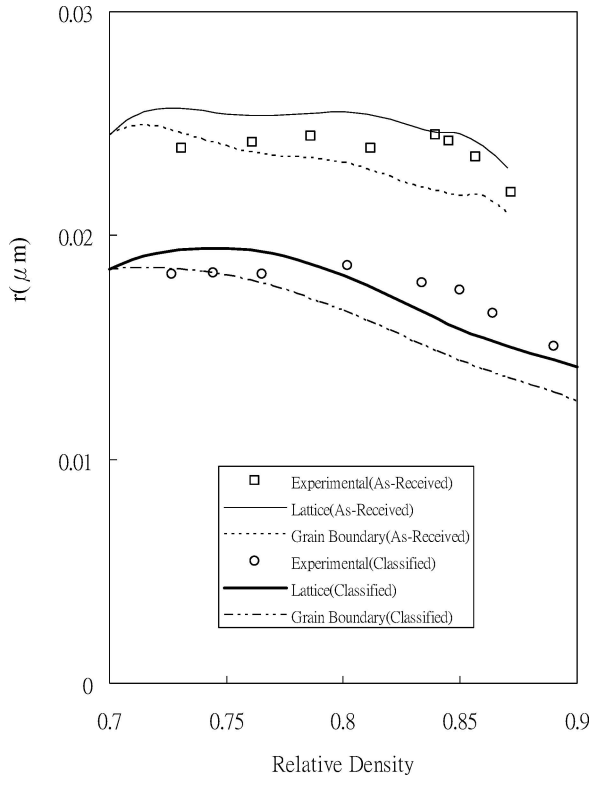

Figure 1 Comparison of the experimental and the evaluated values of the average pore radius (r) of as-received and classified powder compacts.

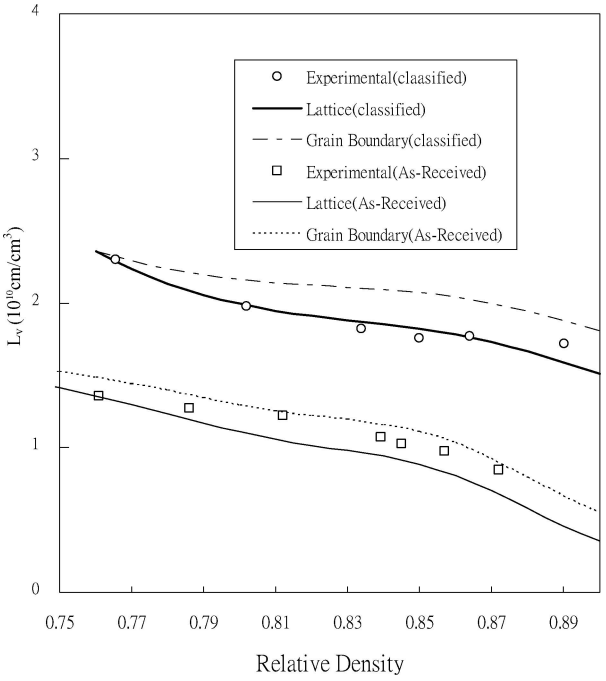

Figure 2 Comparison of the experimental and the evaluated values of the total length of pore channels per unit volume (L_v) of as-received and classified powder compacts.

Fig. 4 shows the comparison of the open pore population in volume percentage for as-received and classified powder compacts. Pores start to pinch off at 91% relative density for the classified powder compact but at 86% relative density for the as-received one.

Fig. 5 shows the comparison of the sintering behaviors, at a heating rate of 10°C/min, for the undoped, MgO-doped, and ZrO_2-doped powder compacts. It was found that the sintering temperature was increased by adding the dopants, and ZrO_2-doped powder compacts had the highest sintering temperature. Fig. 6 shows comparisons of the densification rate versus density for the undoped, MgO-doped, and ZrO_2-doped alumina compacts.

It has been suggested [63] that an impurity segregating to the grain boundaries inhibits grain-boundary diffusion, which, in turn, causes lattice diffusion to dominate. And, as mentioned above, for undoped compacts, the evaluated data with lattice diffusion have a better fit to the experimental data. Therefore, in Figs 7–9, only the lattice diffusion of aluminum ion was selected for evaluating the morphological parameters of microstructural evolution of the MgO-doped and

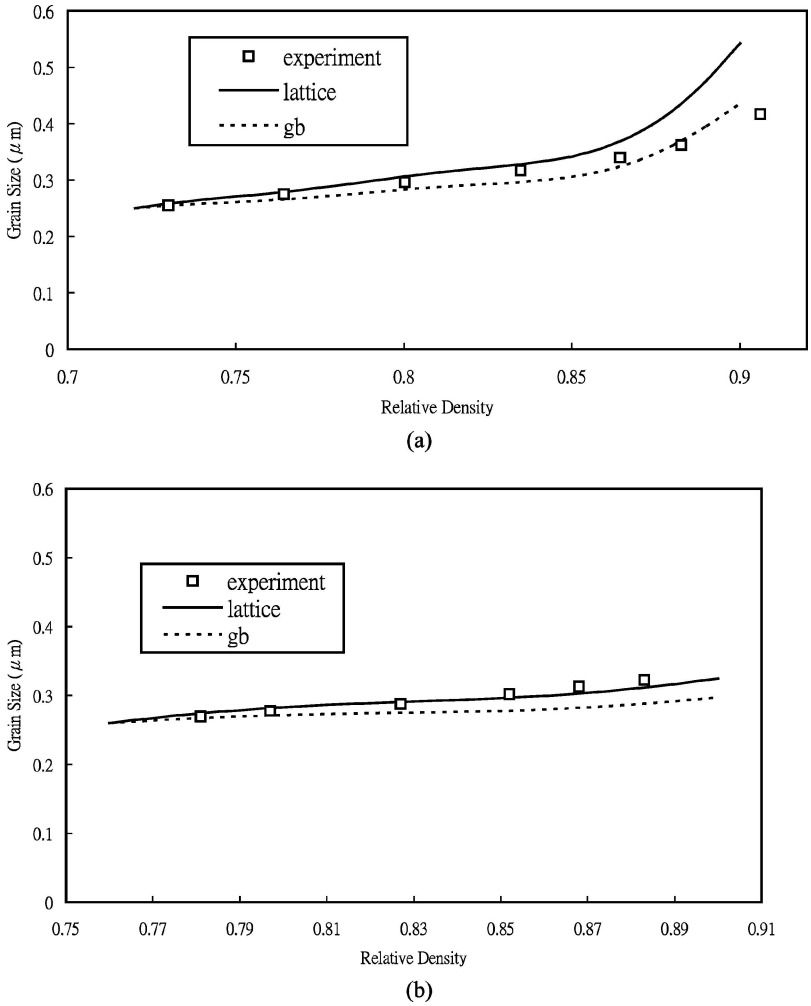

Figure 3 Comparison of the experimental and the evaluated values of the average grain size of (a) as-received and (b) classified powder compacts.

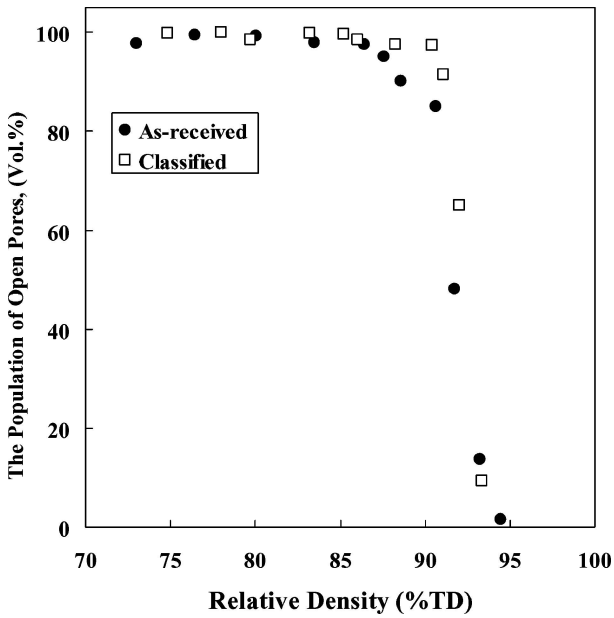

Figure 4 Comparison of open-pore population (in vol%) for as-received and classified powder compacts.

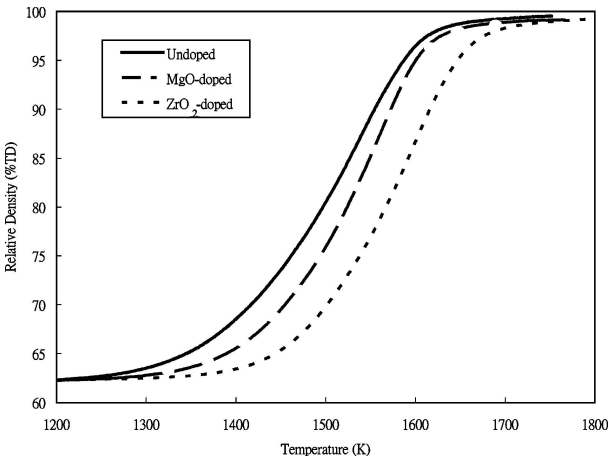

Figure 5 Comparison of the sintering behavior at a heating rate of 10°C/min for undoped, MgO-doped, and ZrO_2-doped alumina compacts.

ZrO_2-doped alumina compacts. This point is also supported by the high evaluated activation energies, i.e., 790 ± 23 KJ/mol and 956 ± 42 KJ/mol for MgO- and ZrO_2-doped alumina compacts, respectively [60]. Moreover, the reference data line of the undoped compact was based on the regression of the experimental data of the classified, undoped alumina powder compact and the onset points of both doped samples were taken the same as that of the undoped sample. Fig. 7 shows a comparison of r values at different density levels for the undoped, MgO-doped, and ZrO_2-doped alumina compacts. For the doped compacts, they exhibited the same trend, i.e., the decrease in r over the whole density range but the shrinking rate of r of the

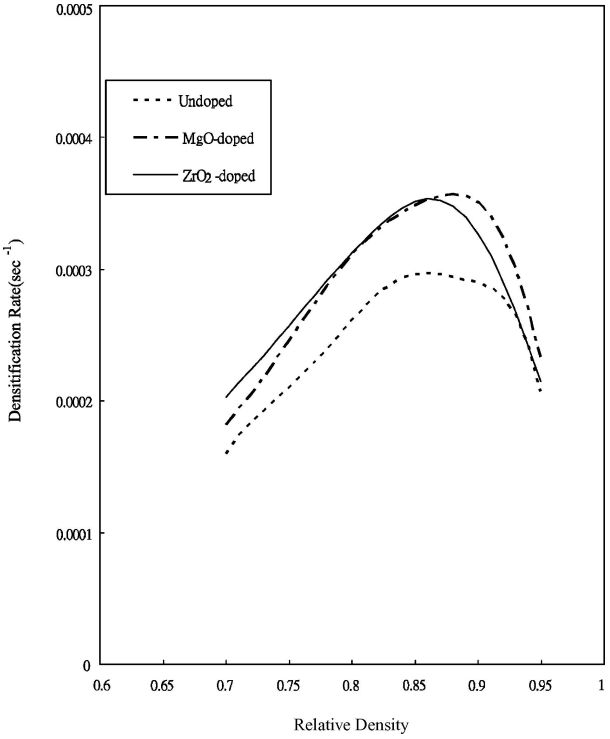

Figure 6 Comparisons of densification rate versus relative density for undoped, MgO-doped, and ZrO_2-doped alumina compacts at a heating rate of 10°C min^{-1}.

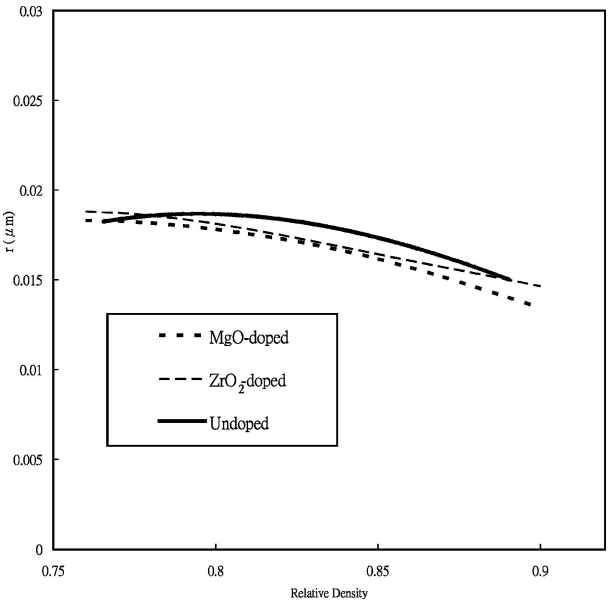

Figure 7 Comparison of the average pore radius (r) at different density levels for undoped, MgO-doped, and ZrO_2-doped alumina compacts.

ZrO_2-doped compact seems to be suppressed at relative densities >86%.

Fig. 8 shows the comparison of L_v values at different density levels for the undoped, MgO-doped, and ZrO_2-doped alumina compacts. As observed, the L_v of these compacts remained essentially steady at relative densities <86%, but that of the ZrO_2-doped compact decreased quickly at relative densities >86%.

Fig. 9 shows the evolution of grain size at different relative densities. The grain size increased with the increase of the density for these compacts. Although the ZrO_2-doped compact had the smallest grain sizes

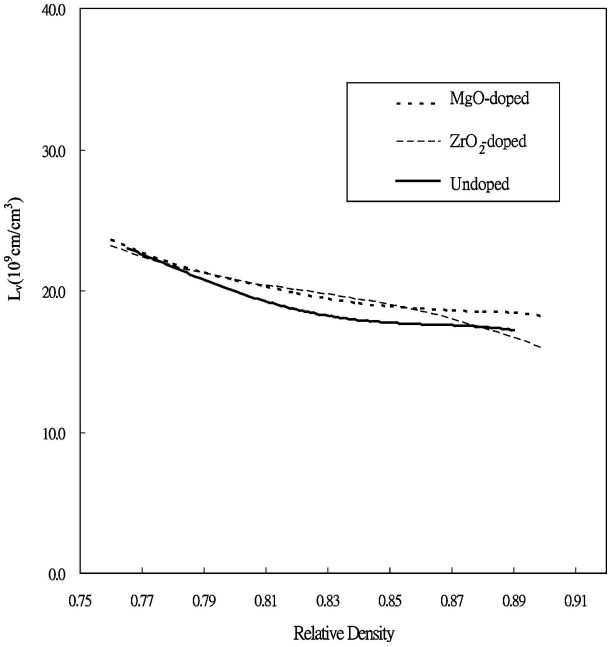

Figure 8 Comparison of the total length of pore channels per unit volume (L_v) at different density levels for undoped, MgO-doped, and ZrO_2-doped alumina compacts.

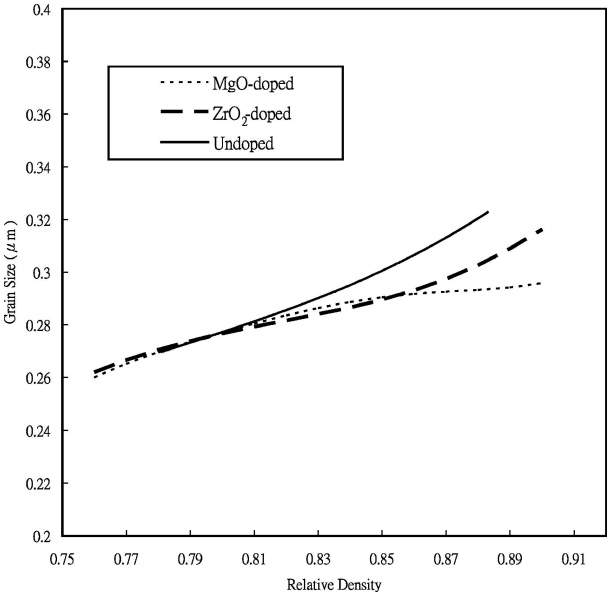

Figure 9 Comparison of the average grain size at different density levels for undoped, MgO-doped, and ZrO_2-doped alumina compacts.

at relative densities <86%, the grain size of the MgO-doped compact became the smallest at relative densities >86%.

4. Discussion

The key issue of the intermediate stage of sintering is to realize the morphological changes of pore channel network. The former treatments were mostly to consider a fixed geometry with constant connectivity, unchanging particle coordination and with uniform shrinking until porosity drops to less than 10% where suddenly the pores become unstable and disconnect. Prochazka [64] argued that the sintering bodies possess catenoid-like surfaces rather than long cylinders and the connectivity

is reduced continuously during sintering until it is zero at which point the pores form a chain. He illustrated a soap film stretched between two wire loops and further suggested that the pinch-off of the pore channels occurs at a critical separation where the surface area of the catenoidal surface is equal to that of the two loops. Fig. 3 shows that the 100% open pores remains until 91 and 86% relative densities for the classified and as-received powder compacts, respectively, thereafter, there is a quite sharp transition from the continuous pore channels to isolated pores for both powder compacts. Therefore, the pore channels do not pinch off continuously as suggested by Prochazka [64]. Based on an ideal structure, Budworth [65] proposed a simple criterion, which essentially is the same as that of the zero growth rate in the perturbation phenomena of the Rayleigh instability [19], to predict the critical porosity for the sudden breakup of all the pore channels. The calculated value of the critical porosity is in reasonable agreement with the experimental data shown in Fig. 4. Thus, the perturbation phenomena of Rayleigh instability [19–27] may indeed play a role in the development of closed pores in powder compacts undergoing densification.

In Fig. 2, for the as-received powder compact, the quick decrease of L_v at relative densities >86% corresponds to the region of the gradual reduction of open pores in Fig. 4, indicating that the values of L_v are related to the closure of the pore channels. The early breakup of some pore channels may be due to the effect of particle size distribution, which can be rationalized that according to the theory of perturbation phenomena of the Rayleigh instability [19–27], any nonuniformity and accidental fluctuation in the pore cross section would cause the possible breakup of pore channels, therefore, the vicinity of the nodes (corners or four-grain junctions) basically a natural perturbation could be affected by the particle size distribution and cause early breakup of some channel pores.

In Fig. 8, it is interesting to point out that L_v of the MgO-doped sample has the same trend as the undoped classified one, i.e., L_v values basically remain steady for relative densities above 82% but those of ZrO_2-doped samples remain essentially steady below 86% and decrease quickly above 86%. As mentioned above, for the as-received powder compact, it implies that there is breakup of some pore channels at relative densities above 86% for ZrO_2-doped samples. Because the same classified powder was used for the undoped and doped samples, there are factors other than particle size distribution to make L_v different. Drory and Glaeser [25] suggested that in a compact, if mass redistribution along the pore channel occurred rapidly in comparison to the pore channel shrinkage, pore closure as a result of the growth of morphological perturbation might become possible. This implies that the mass redistribution via surface diffusion would lend support to avoiding the early breakup of pore channels. Because the temperature and impurity can modify the diffusion mechanisms, they would have an influence on the breakup of the pore channels. For ZrO_2-doped samples, the very high sintering temperature would promote the radius shrinkage of the pore channel and be harmful to the stability of the pore channels. Though the sintering temperature of MgO-doped sample is also high, its L_v values still maintain steady as the same trend of undoped one, which may be due to the enhancement of the surface diffusion [6, 26] magnifying the mass redistribution. However, more works need to be done to clarify this mechanism.

In Fig. 5, it is observed that the sintering temperature of the ZrO_2-doped alumina compacts is the highest among these three compacts at the same density level. However, Fig. 7 reveals that at relative densities in a range from 80% to 86%, the r values of both doped compacts are very close, whereas at relative densities >86%, the r values of the ZrO_2-doped alumina compact become larger. Thus, the suppression of the shrinking rate of the pore radius for the ZrO_2-doped alumina compact at relative densities >86% needs to be rationalized. Because the densification rate depends on the grain size, density, and temperature, it would be difficult to assess the effect of impurity on the densification behavior if one of these factors is not fixed. Fortunately, owing to the small difference of the grain sizes for the doped samples (Fig. 9), it becomes possible to interpret this effect based on density and temperature. At relative densities >86%, because the sintering temperature of ZrO_2-doped alumina compacts is higher than MgO-doped samples (Fig. 5), the densification rate of ZrO_2-doped samples shown in Fig. 6 is indeed lower than that of the MgO-doped ones at a given density, which could be attributed to the densification rate enhanced by MgO [1] or reduced by ZrO_2 [54]. Because the enhancement of the densification rate by MgO dopant is still under controversy [4, 37], the latter may be favorable to explain the suppression of the shrinking rate of the pore radius for the ZrO_2-doped alumina compact.

Based on the results of undoped samples (Figs 1–3), the rapid enhancement of the grain growth is dominated by the change of L_v rather than r in the intermediate stage of sintering. In Fig. 9, though ZrO_2-doped samples have the lowest grain sizes at relative densities <86%, the grain sizes of the MgO-doped samples become lowest when relative densities >86%. This result could take two factors related to the drag of the grain boundary into account, i.e., impurity and pore. It is suggested that Zr^{4+} has more effective impurity drag in inhibiting grain growth [54] but at relative densities above 86%, the grain growth rate of MgO-doped sample become lower, which can be attributed to the great help of pore drag because its pore channel network remains continuous.

5. Conclusions

(1) The modified statistical theory is further justified as valid for evaluating microstructural parameters, i.e., average pore radius, grain size, and total length per unit volume of pore. These evaluated data of microstructural parameters provide deep insight of the effects of particle size distribution and dopants on the sintering behaviors of the powder compacts.

(2) Particle size distribution has more influence on L_v than other parameters and nonuniform particle

size distribution would cause early breakup of pore channel.

(3) MgO-doped samples can maintain a steady L_v of pore channels as the classified powder compact. It indicates that the 100% open pores can be remained until a higher critical density for the breakup of the pore channel, which may be due to the enhancement of the surface diffusion by MgO dopant and would do a great favor to inhibit the grain growth.

(4) ZrO_2 dopant can suppress the shrinking rate of the pore radius and is more effective in inhibiting the grain growth, but the increase of the high sintering temperature would cause the early breakup of the pore channels, indicated by the quick reduction of L_v.

Acknowledgment

Supported by the National Science Council of Taiwan, the Republic of China, under Contract No. 81-0405-E006-15.

References

1. R. L. COBLE, *J. Appl. Phys.* **32** (1961) 787.
2. R. J. BROOK, *J. Am. Ceram. Soc.* **52** (1969) 56.
3. M. F. YAN. *Mater. Sci. Eng.* **48** (1981) 53.
4. M. P. HARMER, "in Advances in Ceramics," edited by W. D. Kingery (The American Ceramic Society, Columbus, OH, 1984) Vol. 10, p. 679.
5. R. E. MISTLER and R. L. COBLE, *J. Am. Ceram. Soc.* **51** (1968) 237.
6. K. A. BERRY and M. P. HARMER, *ibid.* **69** (1986) 143.
7. N. J. SHA and R. J. BROOK, *ibid.* **69** (1986) 107.
8. C. H. HSUEH, A. G. EVANS and R. L. COBLE, *Acta Metall.* **30** (1982) 1269.
9. M. A. SPEARS and A. G. EVANS, *ibid.* **30**, 1281.
10. R. J. BROOK, E. GILBART, N. J. SHAW and U. EISELE, *Powder Metall.* **28** (1985) 105.
11. J. RODEL and A. M. GLAESER, *J. Am. Ceram. Soc.* **73** (1990) 3302.
12. F. S. SHIAU, T. T. FANG and T. H. LEU, *ibid.* **80** (1997) 286.
13. R. L. COBLE and T. K. GUPTA, "in Sintering and Related Phenomena," edited by G. C. Kuczynski, N. A. Hooton and C. F. Gibbon (Gordon and Breach, NY, 1967) p. 423.
14. W. BEERE, *Acta Metall.* **23** (1979) 131.
15. R. M. GERMAN, *J. Am. Ceram. Soc.* **61** (1978) 272.
16. D. L. JOHNSON, *ibid.* **53** (1970) 574.
17. F. N. RHINES and R. T. DEHOFF, "in Materials Science Research," edited by G. C. Kuczynski and A. E. Miller (Plenum Press, NY, 1984) Vol. 16, p. 49.
18. T. T. FANG and H. PALMOUR III, *Ceram. Int.* **15** (1989) 329.
19. L. RAYLEIGH, *Proc. London Math. Soc.* **10** (1879) 4.
20. F. A. NICHOLS and W. W. MULLINS, *Trans. A. I. M. E.* **233** (1965) 1840.
21. *Idem., J. Appl. Phys.* **36** (1965) 1826.
22. F. A. NICHOLS, *J. Mater. Sci.* **11** (1976) 1077.
23. J. W. CAHN, *Scripta Metall.* **13** (1979) 1069.
24. W. C. CARTER and A. M. GLAESER, *J. Am. Ceram. Soc.* **67** (1984) C124.
25. M. D. DRORY and A. M. GLAESER, *ibid.* **68** (1985) C14.
26. J. D. POWERS and A. M. GLAESER, *ibid.* **75** (1992) 2547.
27. L. KULINSKY, J. D. POWERS and A. M. GLAESER, *Acta Mater.* **44** (1996) 4115.
28. T. T. FANG and H. PALMOUR III, *Ceramics International*, **16** (1990) 63.
29. T. T. FANG and H. L. HSIEH, *J. Mater. Sci.* **27** (1992) 4639.
30. P. D. S. ST. PIERR and A. GATTI, U. S. Patent # 3,026,177 March 1962.
31. R. L. COBLE and J. E. BURKE, *Progr. Ceram. Sci.* **3** (1963) 197.
32. J. E. BURKE, *J. Am. Ceram. Soc.* **40** (1957) 80.
33. R. L. COBLE, *ibid.* **45** (1962) 123.
34. C. A. BRUCH, *Am. Ceram. Soc. Bull.* **41** (1962) 799.
35. D. L. JOHNSON and I. B. CUTLER, *J. Am. Ceram. Soc.* **46** (1963) 545.
36. P. J. JORGENSEN and J. H. WESTBROOK, *ibid.* **47** (1964) 332.
37. P. J. JORGENSEN, *ibid.* **48** (1965) 207.
38. M. O. WARMAN and D. W. BUDWORTH, *Trans. Brit. Ceram. Soc.* **6** (1967) 253.
39. R. J. BROOK, *Scripta Metall.* **2** (1968) 375.
40. S. K. ROY and R. L. COBLE, *J. Am. Ceram. Soc.* **51** (1968) 1.
41. D. W. BUDWORTH, *Mineral. Mag.* **37** (1970) 833.
42. N. A. HAROUN and D. W. BUDWORTH, *Trans. Brit. Ceram. Soc.* **69** (1970) 73.
43. S. S. C. TONG and J. P. WILLIAMS, *J. Am. Ceram. Soc.* **53** (1970) 58.
44. I. D. PRENDERGAST, D. W. BUDWORTH and N. H. BRETT, *Trans. Brit. Ceram. Soc.* **71** (1972) 31.
45. H. L. MARCUS and M. E. FINE, *J. Am. Ceram. Soc.* **55** (1972) 568.
46. A. MOCELLIN and W. D. KINGERY, *ibid.* **56** (1973) 309.
47. P. J. JORGENSEN, in Proceedings of the 4th. Bolton Landing Conference, edited by J. L. Walter, J. J. Westbrook and D. A. Woodford (Claitor Publishing Division, Baton Rouge LA, 1974) p. 205.
48. R. I. TAYLOR, J. P. COAD and R. J. BROOK, *J. Am. Ceram. Soc.* **57** (1974) 539.
49. J. G. J. PEELAN, *Mater. Sci. Res.* **10** (1975) 443.
50. W. C. JOHNSON and D. F. STEIN, *J. Am. Ceram. Soc.* **58** (1975) 485.
51. W. C. JOHNSON, *Metall. Trans. A.* **8A** (1977) 1413.
52. S. J. BENNISON and M. P. HARMER, in "Ceramic Transactions," edited by C. A. Handwerker, J. E. Blendell and W. Q. Kaysser (American Ceramic Society, Westerville, OH, 1990) Vol. 7, p. 13.
53. F. A. KROGER, *J. Am. Ceram. Soc.* **67** (1984) 390.
54. R. MAJUMDAR, E. GILBART and R. J. BROOK, *Br. Ceram. Trans J.* **85** (1986) 156.
55. F. F. LANGE, T. YAMAGUCHI, B. I. DAVIS and P. E. D. MORGAN, *J. Am. Ceram. Soc.* **71** (1988) 446.
56. J. WANG and R. RAJ, *ibid.* **73** (1990) 1172.
57. *Idem., ibid.* **74** (1991) 1959.
58. "Standard Methods for Determining the Average Grain Size," ASTM Designation E112-82, Annual Book of ASTM Standards, American Society for Testing and Materials, Philadelphia, PA, 1983 Vol. 03, p. 121.
59. C. ZENER, *Trans. Am. Inst. Min. Engrs* **47** (1948) 175.
60. F. S. SHIAU, Ph.D. Dissertation, National Cheng Kung University, 2001.
61. T. T. FANG, F. S. SHIAU and J. T. SHIUE, *Mater. Chem. and Phys.* 9630 (2002) 1.
62. R. M. CANNON, W. H. RHODES and A. H. HEUER, *J. Am. Ceram. Soc* **63** (1980) 46.
63. T. DOSDALE and R. J. BROOK, *ibid.* **66** (1983) 392.
64. S. PROCHAZKA, in "Ceramic Transactions," edited by C. A. Handwerker, J. E. Blendell and W. A. Kaysser (The American Ceramic Society, OH, 1990) Vol. 7, p. 164 .
65. D. W. BUDWORTH, *Trans. Brit. Ceram. Soc.* **69** (1970) 29.

Received 23 October 2003
and accepted 19 October 2004